An Electrochemical Investigation of the Impact of Microfabrication Techniques on Polymer-Based Microelectrode Neural Interfaces

Seth A. Hara, *Student Member, IEEE*, Brian J. Kim, Jonathan T. W. Kuo, and Ellis Meng, *Senior Member, IEEE*

***Abstract*— The electrochemical (EC) properties of microelectrodes on flexible polymer substrates can vary as a result of microfabrication and postfabrication processes. These in turn may impact the chronic recording performance of such electrodes. In this paper, electrochemical techniques were utilized for the preparation and nonbiological evaluation of microfabricated flexible neural probes consisting of platinum electrode recording sites supported and insulated by Parylene C. The polymer substrate mitigates the mechanical mismatch between neural tissue and the probe. In addition, the thermoplastic nature of the polymer enables the probe to be shaped postfabrication using a thermoforming technique to impart a unique 3-D structure that further promotes tissue integration and supports the use of bioactive coatings. The EC techniques provided a simple means to clean electrode surfaces (80.2% decrease in 1-kHz impedance), identify functional devices, and evaluate their EC properties prior to implant. Both electrochemical impedance spectroscopy and cyclic voltammetry measurements were performed on electrode sites following fabrication, cleaning, mechanical manipulation for assembly, thermoforming, and sterilization. The results reveal in some cases changes in EC properties. Although changes following thermoforming did not impact the ability to acquire electrophysiological recordings, further investigation with additional tools is required to elucidate the exact nature of the structural and EC changes resulting in the observed increase in impedance and reduction in electrode surface area following thermoforming. [2014-0378]**

***Index Terms*— Brain-computer interface, cyclic voltammetry, electrochemical impedance spectroscopy, microelectrodes, neural microtechnology, neural prosthesis.**

I. Introduction

CHRONIC intracortical recording reliability continues to be a challenge in the design of neural prostheses. In addition to nonbiological failure mechanisms such as delamination of insulation, electrode breakage, or electrode corrosion, current probe technology is susceptible to biological failures which are believed to arise from immune response to the presence of foreign material. Insertion trauma to the neural tissue [1] and blood-brain barrier [2], chronic presence of a foreign body in the tissue [1], [3]–[5], and the associated chronic aggravation arising from the mechanical mismatch between brain tissue and traditional rigid probes [6]–[8] have all been linked to biological failures.

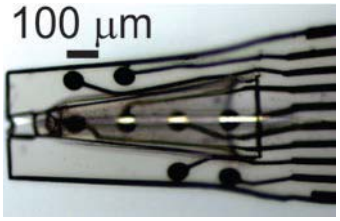

Fig. 1. Optical micrograph of the PSE, showing the placement of four electrodes inside of the sheath and four on the periphery.

One tactic to mitigate biological failure is through the use of materials, such as polymers, with low Young's moduli to better match the mechanical properties of brain tissue and alleviate the chronic irritation that mechanical mismatch can cause [6]–[8]. A different approach promotes dendritic growth through the use of bioactive molecules to reduce the distance between the signal source and recording sites [3], [9], [10]. Both of these strategies were implemented in the Parylene Sheath Electrode (PSE; Fig. 1), an intracortical neural probe fabricated on a Parylene C substrate. The PSE consists of a three-dimensional (3D) open-lumen sheath structure with four electrode sites situated on the interior surface of the sheath and four on the outer periphery, thereby leveraging the neurotrophic electrode (NE) approach invented by Kennedy *et al.* [10], while also capitalizing on the benefits of batch microfabrication using a thin-film polymer.

Microfabricated polymer probes may undergo unique processing compared to their silicon and ceramic counterparts. This in turn may impact recording quality and should be evaluated. Detailed characterization of electrodes is not often reported, which restricts the long-term impact of such technologies. Many groups have demonstrated the use of polyimide, an encapsulant commonly used in the microelectronics industry, to create neural probes with multiple metal layers and high electrode densities [11]–[14]. The probes are formed by sandwiching thin-film metal between layers of polyimide and selectively exposing the electrode sites. Another commonly used material, Parylene C (hereto referred

Manuscript received December 12, 2014; revised March 16, 2015; accepted May 7, 2015. Date of publication June 1, 2015; date of current version July 29, 2015. This work was supported by the Defense Advanced Research Projects Agency Microsystems Technology Office through the Space and Naval Warfare Systems Center under Contract N66001-11-1-4207. Subject Editor C. Ahn.

The authors are with the Department of Biomedical Engineering, University of Southern California, Los Angeles, CA 90089 USA (e-mail: sethhara@usc.edu; brianjk@usc.edu; jonathtk@usc.edu; ellismen@usc.edu).

Color versions of one or more of the figures in this paper are available online at http://ieeexplore.ieee.org.

Digital Object Identifier 10.1109/JMEMS.2015.2434827

to as Parylene), is also compatible with standard microfabrication techniques and is often used as both the substrate and insulation material for neural probes [15]–[18]. Parylene is especially of interest for application in neural probes due to its desirable barrier properties, ease of deposition, thermoplastic nature, flexibility (Young's modulus of 4 GPa [19]), mechanical strength, designation as a USP Class VI material, and history of use in Food and Drug Administration (FDA) approved implants [20]. To bring these polymer probe technologies to maturity, it is imperative to fully characterize their properties and understand how their unique processing may affect their application *in vivo.*

Electrochemical (EC) techniques are commonly used to characterize electrode properties for neural probe applications. While EC methods may not be completely conclusive, they are one of the few tools available for evaluation of polymer-based devices prior to implantation. Electrochemical impedance spectroscopy (EIS) provides a measure of the electrode impedance as a function of frequency, a parameter often used to monitor the EC characteristics of the electrode-electrolyte interface, and cyclic voltammetry (CV) is used to electrochemically clean the electrode surface as well as measure an electrode's electroactive area. These tests are typically conducted just prior to implantation to confirm that the electrode properties are well-suited to their intended application, whether that be recording or stimulation [21], but are also powerful tools to investigate probe degradation [22].

The PSE utilizes novel fabrication techniques with potential EC implications on electrode recording performance. As polymer-based neural probes possess the potential to mitigate the chronic irritation to brain tissue [8], [23]–[25], it is necessary to evaluate the impact of fabrication techniques on electrode recording performance and determine suitability of the fabrication techniques for adoption in chronic recording probes. Preliminary characterization of the PSE was presented in a prior study [26]. In this work, electrodes were evaluated by EIS following the complete fabrication of the probe and at each step post-fabrication, including EC cleaning, thermoforming, and sterilization.

II. Methods

A. Fabrication of the Parylene Sheath Electrode

For a complete description of the fabrication process, the reader is referred to our earlier work [27]. The process is briefly summarized here.

The PSE was surface micromachined entirely from Parylene and platinum. 5 μm of Parylene was deposited on a silicon carrier wafer with its native oxide layer intact using a chemical vapor deposition (CVD) process (Fig. 2a). Circular platinum (Pt) electrodes, traces, and contact pads were e-beam deposited (200 nm thick) and patterned through a liftoff process (Fig. 2b). Electrode sites were 45 μm in diameter, which is acceptable for single- and multi-unit recording applications [21]. A 1 μm Parylene layer was deposited to insulate the Pt traces and an O_2 plasma etch exposed the electrode sites and contact pads (Fig. 2c). A final 5 μm layer of Parylene was deposited over a photoresist sacrificial layer

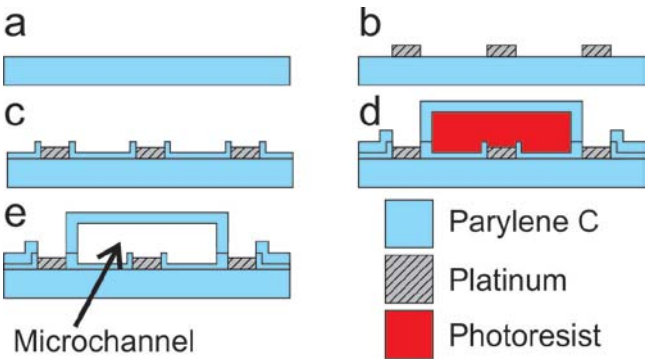

Fig. 2. Cross-sectional illustration of the major fabrication steps for the PSE with exterior electrodes located on the periphery of the sheath. (a) Silicon carrier wafer, (b) patterned platinum electrodes, (c) patterned Parylene insulation, (d) Parylene deposition on photoresist sacrificial layer, and (e) dissolution of sacrificial layer to release microchannel.

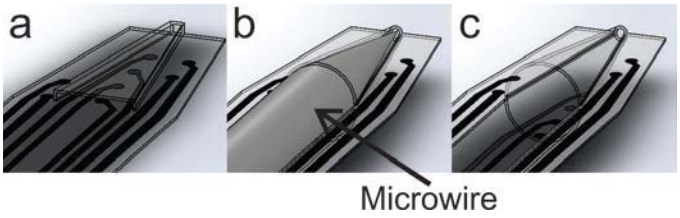

Fig. 3. Illustration of the thermoforming process. A custom-tapered stainless steel microwire was inserted into the flat surface micromachined PSE (a) to fully open the sheath structure (b). Following heat treatment, the microwire was removed and the 3D sheath retained the desired shape (c).

to form the microchannel that becomes the sheath (Fig. 2d). The electrode sites, contact pads, and both sides of the Parylene microchannel were etched with O_2 plasma. Finally, the outline of the PSE was O_2 plasma etched and the PSE was released from the wafer; the presence of the native oxide facilitates the release. The sacrificial layer was removed from the microchannel with an acetone soak (Fig. 2e). The final outline etch was used to create different probe geometries, one conical and the other cylindrical in shape, the purpose of which was to determine an optimal geometry to minimize surgical trauma during implantation.

To create the 3D sheath, the flat microchannels were molded by a thermoforming process (Fig. 3); the same process also improves the adhesion between the multiple Parylene layers [28], [29]. First, custom-tapered stainless steel microwires were inserted into the microchannel. With the microwires in place, the wire-channel assemblies were annealed at 200 °C for 48 hours under vacuum. The temperature was then slowly ramped down to room temperature and the microwires were removed, leaving the 3D sheaths in the desired shape. This heat treatment process alters the crystallinity of the Parylene, allowing it to permanently adopt the shape of its mold [30].

B. Ethylene Oxide Sterilization

In a concurrent *in vivo* study, the PSE was sterilized with ethylene oxide (EtO) prior to implantation. To determine the EC effects of this process, the PSE was EC tested before and after sterilization. Sterilization was performed at room temper-

ature with the Anprolene AN74i sterilizer system (Andersen Products, Inc., Haw River, NC) using a 24 hour cycle.

C. Electrochemical Techniques

CV was used to both provide a measure of the electroactive surface area and to produce a clean electrode surface prior to further testing. EIS was then used to measure the electrode impedances at various points of the fabrication process. To conduct the EC measurements, a Gamry Reference 600 potentiostat (Gamry Instruments, Warminster, PA) was used with a Faraday cage to minimize noise. To overcome the hydrophobicity of Parylene that prevents the filling of the probe's conical sheath structure, the Parylene surface was first wetted with isopropyl alcohol prior to immersion in the measurement solution. Each electrode was subjected to a single experimental trial in each sample set.

In addition to standard microfabrication cleaning techniques (repeated rinses with acetone, isopropyl alcohol, and deionized water), CV was used to electrochemically clean the electrode surface, as described by Petrossians *et al.* [31]. This provides the same oxidation/reduction process as voltage pulsing used in other EC disciplines [32]–[37], but in a less aggressive manner. Using a three-electrode cell, electrodes were immersed in 0.05 M H_2SO_4 with constant N_2 purging. The working electrode was cycled between -0.2 to 1.2 V with respect to an Ag/AgCl (3M NaCl) reference, a potential range that is within the water window [38]. A 1 cm^2 Pt plate served as the counter electrode. Using a scan rate of 250 mV/s, each electrode was cycled for 30 cycles at which point the curves reached a steady-state, indicating that no further cleaning was occurring.

EIS was performed in phosphate buffer saline ($1\times$ PBS) at 37 °C with an AC perturbation signal of 10 mV_{rms} in the frequency range of 1-10^5 Hz. As with CV, an Ag/AgCl (3M NaCl) reference and 1 cm^2 Pt plate counter were used.

The well-understood redox behavior of the ferricyanide/ferrocyanide couple was utilized to investigate the possibility that thermoforming obscures the electrode surface, which may account for the observed electrochemical changes in the EIS and CV results. This redox couple is often used with CV as it is a relatively uncomplicated model of a highly reversible reaction [39]. To this end, a CV in freshly-prepared 6 mM potassium ferrocyanide ($K_4[Fe(CN)_6]$) was conducted with a scan rate of 50 mV/s from -0.1 to 0.5 V vs. Ag/AgCl with a 1 cm^2 Pt plate counter electrode.

III. Results

A. Electrochemical Cleaning

EC cleaning of the electrodes produced CV curves such as the one seen in Fig. 4. By integrating the hydrogen desorption portion of the curve and utilizing the commonly accepted conversion factor of 210 $\mu C/cm^2$ [40], the electroactive surface area of the curve was calculated to be 19,567 μm^2. The geometric surface area of the electrodes was 1590 μm^2, suggesting a roughness factor of 12.

EIS measurements were taken on pre-thermoformed probes both prior to and after being EC cleaned. As was observed by Grand *et al.* [37], electrode impedance decreased (Fig. 5 and Fig .6). The initial cleaning procedure resulted in a 1 kHz impedance magnitude drop of 80.2% (Table 1),

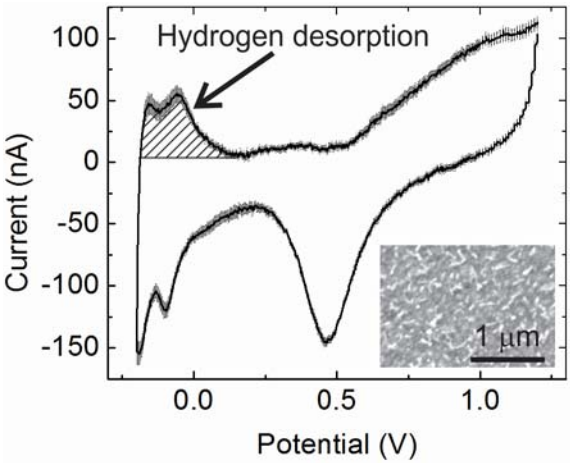

Fig. 4. Representative CV of probe following microfabrication. Mean ± SE, n = 8 electrodes on a single cylindrical sheath geometry probe. Inset: SEM of electrode surface, showing native roughness.

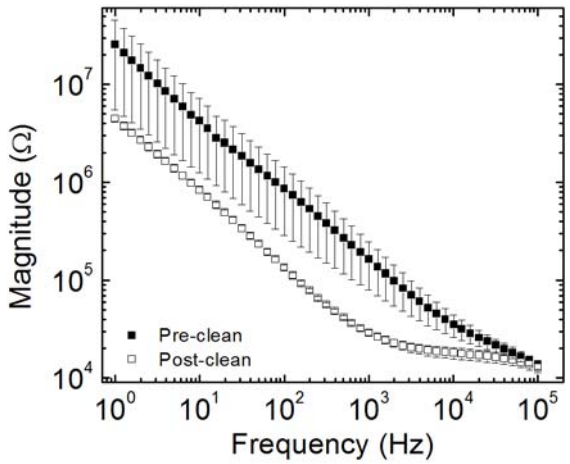

Fig. 5. EIS magnitude plot both prior to (black) and after white) electrochemical cleaning. Data was taken before thermoforming. Cylindrical sheath geometry. Mean ± SE, n = 40 electrodes on 5 probes.

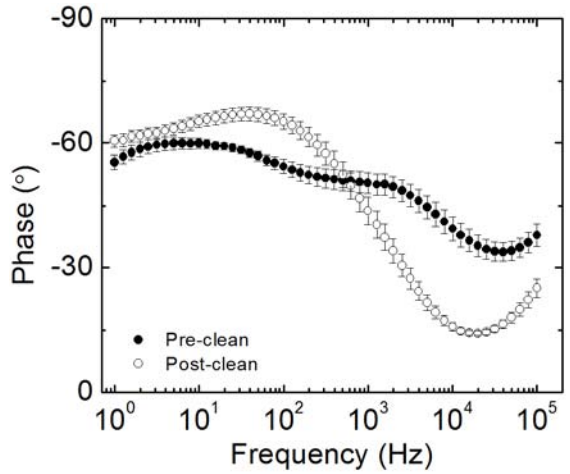

Fig. 6. EIS phase plot both prior to (black) and after (white) electrochemical cleaning. Data was taken before thermoforming. Cylindrical sheath geometry. Mean ± SE, n = 40 electrodes on 5 probes.

TABLE I
COMPARISON OF 1 kHz IMPEDANCE MAGNITUDE VALUES BEFORE AND AFTER ELECTROCHEMICAL CLEANING. CYLINDRICAL SHEATH GEOMETRY, PRE-THERMOFORM: N = 40 ELECTRODES ON 5 PROBES

Condition	*Impedance Magnitude (kΩ)*	*Standard Error (kΩ)*	*Impedance Reduction*
Pre-clean	144.3	405.7	---
Post-clean	28.6	18.2	80.2%

variation between electrodes was reduced, discontinuities observed in the phase curve were removed, and the expected impedance response was obtained.

B. Mechanical Opening of Sheath

The formation of the 3D sheath structure required mechanical opening of the initially flat microchannel with a custom-tapered microwire followed by an annealing process. Mechanically opening the microchannel temporarily formed the sheath, but deformation returned the sheath to its initial flat shape. The mechanical opening step was studied with EIS once the microwire was removed, but prior to any deformation, to confirm that the expansion of the microchannel did not adversely impact EC performance of the electrodes. As the placement of the electrodes either inside of the sheath or on the periphery can also alter their EC performance, the effects of mechanically opening the sheath were studied on each group separately. As can be seen in Fig. 7, the outer electrodes were unaffected by opening of the sheath. The inner electrodes (Fig. 8) exhibit a slight decrease in impedance, likely due to the widening of the conductive path to the counter electrode following expansion of the sheath structure. Similar results are expected in different geometries. The cylindrical sheath geometry has an internal sheath volume that is 122% larger than the conical sheath geometry and the impedance change due to mechanical opening of the sheath is expected to scale accordingly, that is, a larger internal sheath volume correlates to a larger conductive path and thus lower solution resistance.

C. Heat Treatment

Upon EC testing of the PSE following thermoforming, it was discovered that the process significantly changed the EC properties of the electrodes (no significant difference under optical or electron microscopy observation). As seen in Fig. 9, the impedance magnitude of the electrodes after the heat treatment process is greater at lower frequencies and changes slightly in slope. The impedance phase (Fig. 10) shifted towards lower frequencies and became slightly more negative.

CVs conducted in ferrocyanide revealed a distinct difference in electrode performance between electrodes tested prior to and those tested after undergoing the heat treatment process. As observed in Fig. 11, there was a dramatic drop in current following heat treatment.

D. Effects of Ethylene Oxide Sterilization

Testing before and after the EtO sterilization process showed no impact on the performance of the electrodes (Figs. 12 and 13). The minor differences seen in the EIS curves manifest themselves only at high frequencies, where the solution impedance dominates the system response.

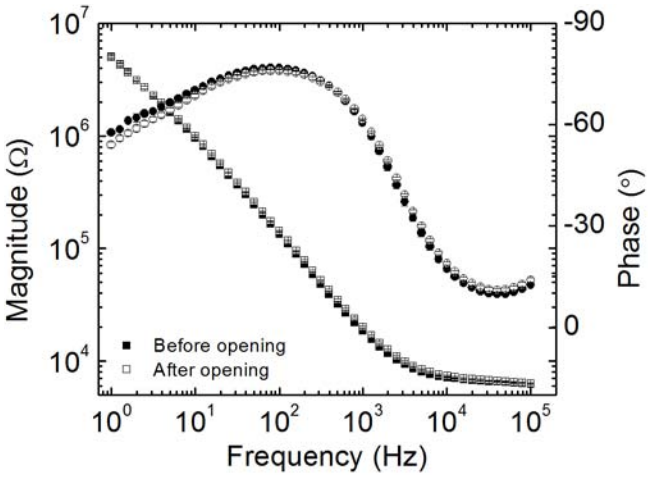

Fig. 7. EIS comparison of outer electrodes before (black) and after (white) mechanically opening the sheath. Magnitude curve is represented by square markers, phase by circles. Cylindrical sheath geometry. Mean ± SE, n = 8 electrodes on 2 probes.

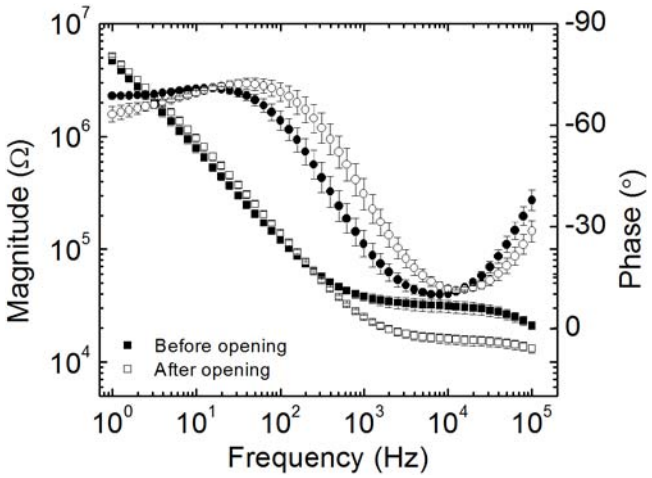

Fig. 8. EIS comparison of inner electrodes before (black) and after (white) mechanically opening the sheath. Magnitude curve is represented by square markers, phase by circles. Cylindrical sheath geometry. Mean ± SE, n = 8 electrodes on 2 probes.

IV. DISCUSSION

In this study, we demonstrated the importance of EC cleaning to produce pristine electrode surfaces for recording. Although microfabricated neural probes have been implanted since 1970 [41], based on research literature, they are not systematically cleaned by electrochemical methods prior to implant. In various other subgenres of electrochemistry, electrochemical cleaning techniques are used to produce clean electrode surfaces. By anodizing the electrode surface and forming an oxide layer, any contaminants that are adsorbed to the electrode surface are removed. Subsequently reducing that oxide layer produces a clean electrode surface [32]. This technique has previously been demonstrated for the *in situ* reduction of bacterial biofouling

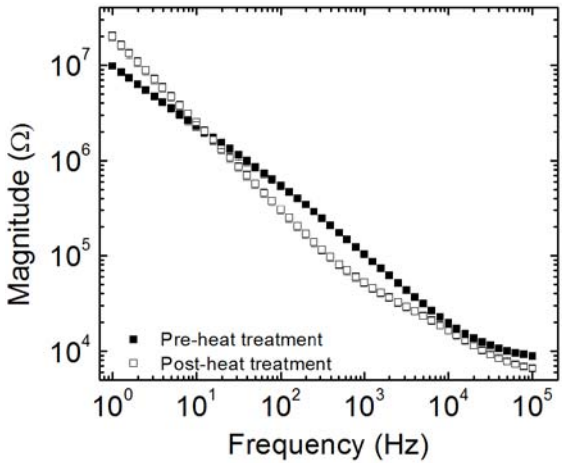

Fig. 9. Impedance magnitude of a PSE before (black) and after (white) heat treatment. Conical sheath geometry. Mean ± SE, n = 15 electrodes on 2 probes.

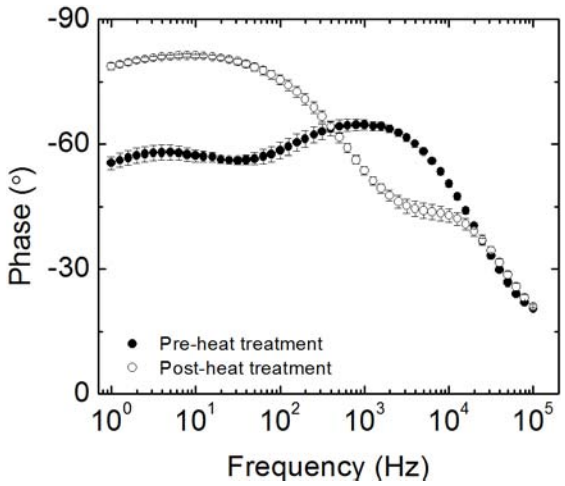

Fig. 10. Impedance phase of the PSE before (black) and after (white) heat treatment. Conical sheath geometry. Mean ± SE, n = 15 electrodes on 2 probes.

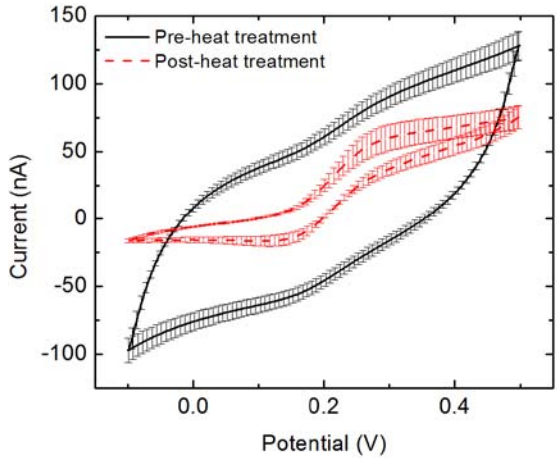

Fig. 11. CVs taken before (black solid line) and after (red dashed line) heat treatment. Conical sheath geometry. Mean ± SE, n=16 electrodes on 2 probes.

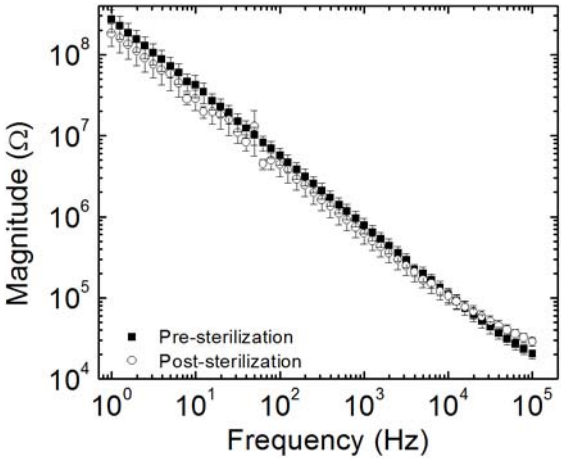

Fig. 12. Impedance magnitude of the PSE before (black) and after (white) sterilization. Conical sheath geometry. Mean ± SE, n = 36 electrodes on 5 probes.

of surfaces in the food and marine industries [33], [34]. For neural probe applications, Otto et al. made a case for rejuvenation of a neural electrode *in vivo* [35] through voltage pulsing, but this technique is designed to mitigate biofouling of the electrode surface and not removal of contaminants prior to implantation. As seen in Fig. 5 and Fig. 6, EC cleaning prior to testing eliminates abnormalities, leading to improved repeatability between devices.

Ulbert et al. mention the use of voltage pulsing to "remove debris from electrode sites possibly built up during storage and sterilization," [36] and this same group later showed a 50% decrease in 1 kHz impedance as a result of this voltage pulsing on a silicon-based neural probe [37]. It was observed that this style of voltage pulsing is potentially destructive for thin-film electrodes on a Parylene substrate, leading to detachment of the electrodes from the Parylene (data not shown). For this reason, CV was used to EC clean the electrode surfaces without damaging them.

Despite the fact that the PSE probes were cleaned with standard microfabrication techniques (and appeared clean by visual inspection under an optical microscope), it was evident that debris, possibly in the form of photoresist scum, remained on electrode surfaces after fabrication, highlighting the importance of this additional EC cleaning step prior to probe implantation. Removal of this debris is critical as the debris obstructs the electrode surface and impedes ion exchange at the electrode-electrolyte interface, thereby attenuating recorded neural signals. These data indicate the importance of additional cleaning of microfabricated electrodes to remove residual contaminants that may obstruct the electrode surface.

In the first generation PSE, the outer electrodes were positioned on top and in the midline of the sheath. The mechanical process used to form the three dimensional sheath exerted a tensile stress on these electrodes in addition to the existing tensile stress imposed on the electrodes as a result of the deposition process [42], [43] and therefore occasionally resulted in electrode cracking. This cracking manifested as increased impedance magnitude of the outer electrodes compared to inner electrodes and shifted phase or multiple time

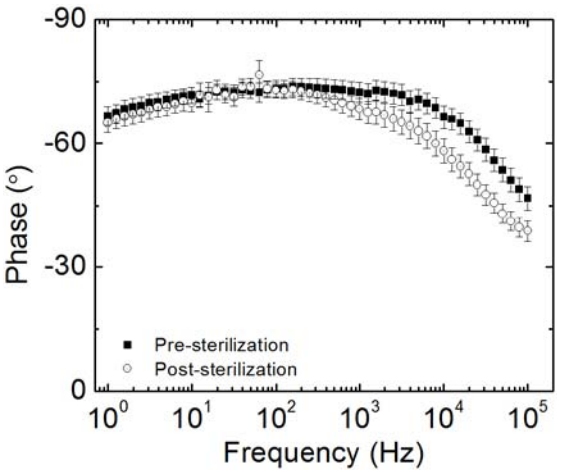

Fig. 13. Impedance phase of the PSE before (black) and after (white) sterilization. Conical sheath geometry. Mean ± SE, n = 36 electrodes on 5 probes.

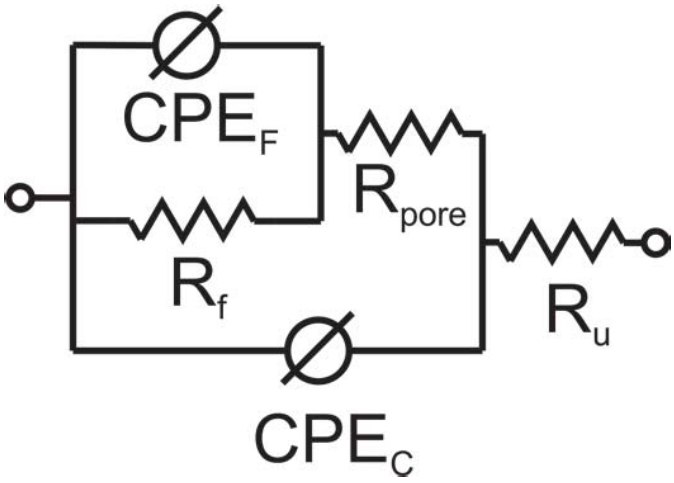

Fig. 14. Equivalent electrical circuit used to model the PSE.

constants in the EIS characterization. Optical microscopy and SEM confirmed the presence of cracks across these electrodes, leading to redesign of the PSE (2^{nd} generation), placing the outer electrodes on the periphery as opposed to the top of the sheath (Fig. 1). This placement could result in improved recordings as the electrodes could benefit from reduced encapsulation and increased proximal neuronal density compared to other locations on the PSE [44].

Although EIS alone is not sufficient to identify electrode cracking on its own, it is a useful tool that may be used in conjunction with microscopy to diagnose this issue unique to 3D polymer-based electrodes. Also, EIS is more amenable to high throughput evaluation of electrode quality and may prove useful as a screening technique for selecting devices suitable for implantation.

The current (2^{nd} generation) PSE design, with the outer electrodes located at the periphery, did not exhibit EC performance differences between inner and outer electrodes following mechanical opening of the sheath. The slight decrease of impedance seen with the inner electrodes was observed at higher frequencies, where the solution impedance is the dominant parameter. This suggests that the impedance decrease may be explained by the widening of the conductive path between the electrode sites and the external Pt counter electrode. The radius of curvature for the conical sheath geometry ranged from 20 μm to 100 μm and was 250 μm for the cylindrical sheath geometry. The placement of the electrodes was such that they only experienced this curvature while under compressive strain. The data indicated that thin-film Pt electrodes in this configuration retain desirable EC characteristics.

The second part of the 3D sheath formation process used in this work, the heat treatment process, has previously been shown to promote adhesion of Parylene layers and improve insulating performance [28], [29]. While the effect of the heat treatment process on exposed electrode sites was not investigated in their work, Rodger et al. demonstrated successful usage of their heat-treated devices *in vivo* to stimulate neurons. In this study, it was found that the process alters the EC properties of the PSE. Although the exact causes of these changes cannot be deduced from these results, a few possibilities are suggested. The increase in impedance observed at low frequencies could indicate a decrease in electrode area, which correlates well with what is observed in the ferrocyanide CV. This could be caused by the deposition or formation of an occluding substance onto the electrode surface during the heat treatment process that is not visible with standard SEM imaging.

Another possible explanation that could contribute to the observed increase in impedance could be the sealing of Parylene layers at exposed interfaces. Prior to heat treatment, it is possible that gaps exist between the Parylene layers due to inadequate adhesion between the layers. As a result, once the devices are immersed, the solution would be in contact with more of the metal surface than intended, producing a lower measured impedance. As the annealing improves the adhesion between the two Parylene layers, these gaps would lessen or disappear, resulting in less metal surface exposed to the solution, and thus, a higher measured impedance. In an attempt to identify the changes occurring at the electrode surface, energy-dispersive X-ray spectroscopy (EDX) and X-ray photoelectron spectroscopy (XPS) measurements were conducted, but proved inconclusive; the penetration depth of the EDX was too great and the spot size of the XPS was too wide to produce a reliable signal just from the electrode surface.

Modeling of the EIS data may help interpret the observed changes. The data sets exhibited two time constants, prompting the use of an equivalent electrical circuit model that includes a coating capacitance in parallel with a simplified Randles circuit (Fig. 14) [45], [46]. This capacitance models the effects of a non-conductive film on the electrode, such as the insulating Parylene layer along the traces of the probe, which may introduce a second time constant to the system. Constant phase elements were used in the model in place of capacitors to better represent the surface inhomogeneities [47]. Modeling software (Echem Analyst,

TABLE II
CALCULATED COMPONENT VALUES FROM MODELED EIS DATA

Component	*Pre-heat treatment*	*Post-heat treatment*
Uncompensated resistance (R_u)	7.5 kΩ	5.8 kΩ
Faradaic resistance (R_f)	111.8 MΩ	698.1 MΩ
Pore resistance (R_{pore})	1.6 MΩ	46.2 kΩ
Faradaic CPE (CPE_f)	19.9×10^{-9} s×s$^{\alpha}$	5.2×10^{-9} s×s$^{\alpha}$
α	0.640	0.930
Equivalent Faradaic capacitance	30.4 nF	5.7 nF
Coating CPE (CPE_C)	9.0×10^{-9} s×s$^{\beta}$	4.5×10^{-9} s×s$^{\beta}$
β	0.799	0.867
Equivalent coating capacitance	3.1 nF	1.2 nF

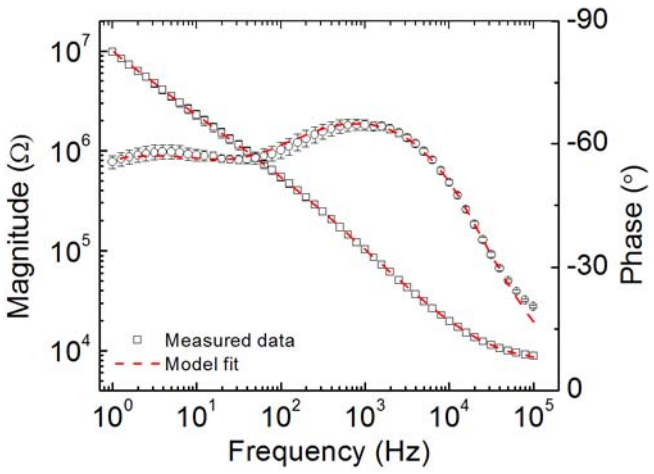

Fig. 15. Pre-heat treatment measured impedance data (magnitude, square markers; phase, circle markers) and model fit (dashed red line).

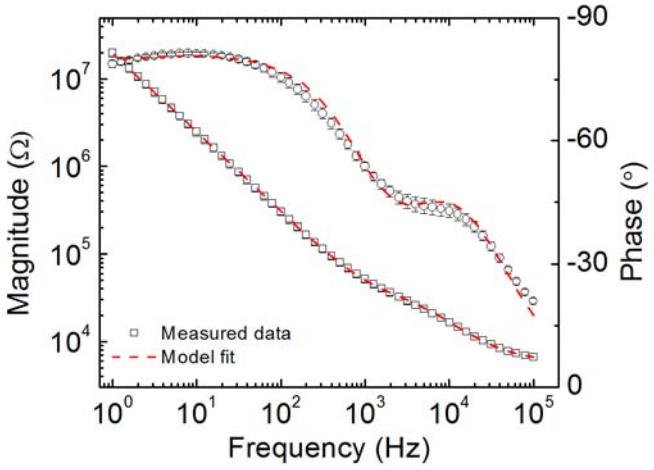

Fig. 16. Post-heat treatment measured impedance data (magnitude, square markers; phase, circle markers) and model fit (dashed red line).

Gamry Instruments, Warminster, PA) was used to calculate the values of the model components, which are detailed in Table 2, and the resulting fits are compared to the data sets in Fig. 15 and Fig. 16.

Based on the model, the changes observed after the heat treatment process are consistent with a sealing of the Parylene layers at the exposed interfaces. The dominant changes occur in the Faradaic resistance, Faradaic capacitance, and the pore resistance components. The increase in Faradaic resistance and decrease in Faradaic capacitance are consistent with a decrease in exposed electrode surface area, as indicated by previous observations, but the value of the Faradaic capacitance may yield an explanation as to what caused the decrease in electrode area. The theoretical capacitance of thin film platinum microelectrodes in physiological saline has been calculated to be 0.545 pF/μm^2 [48]. For our designed electrode area of 1590 μm^2, this equates to a capacitance of 0.9 nF. Although the theoretical calculation does not account for surface roughness, it is expected that the observed electrode roughness would result in a larger capacitance. The Faradaic capacitance modeled from the data approaches the designed theoretical value following heat treatment, suggesting that the exposed electrode surface approaches the desired electrode area. The reduction of R_{pore} further supports this conclusion. Complete removal of this parameter from the model would result in a modified Randles model, a commonly accepted model for a metal electrode in solution, indicating that the sealing of the Parylene layers effectively removes the "pores" that are responsible for the pore resistance element. As this phenomenon is of interest for all Parylene-metal-Parylene devices, new studies are being designed that will further test this hypothesis in test structures. Nonetheless, despite these EC changes, the electrodes successfully obtained neural recordings over the course of a month-long implantation in the rat motor cortex [49]. Longer studies have been completed and the data is under analysis.

Lastly, it was demonstrated that the EtO sterilization process that was used for *in vivo* studies prior to implantation had no effect on the EC performance of the PSE. Minor changes were observed in the EIS curve taken after sterilization, but these changes were isolated to high frequencies where the solution resistance dominates the system response. This change is clearly the result of differences in solution conductivity, due to slight variation in the measurement solution ionic concentration.

V. CONCLUSION

In this work, microfabrication techniques of flexible neural probes were studied through the use of electrochemical methods. An EC cleaning procedure conducted following standard cleanroom cleaning procedures was shown to reduce electrode impedance and correct abnormal impedance performance without causing damage to the electrodes. These results suggest that residue may remain on neural probes from the microfabrication process and that an EC cleaning procedure may be useful in removing such residues prior to implant. EC testing of the PSE indicated that neither the sterilization process nor the mechanical opening of the Parylene microchannel to form the sheath structure had any detrimental effect on the EC performance of the electrodes, provided that the electrodes were not subjected to tensile strain. The heat treatment portion of the thermoforming process, however, resulted in performance variation as the impedance spectra shifted and the current was attenuated in the ferrocyanide CV. It is suspected that the observed EC changes

are due to the sealing of the Parylene layers at the exposed interfaces caused by the heat treatment process, but further work must be conducted to elucidate the mechanisms at play. In spite of these EC variations, as was shown by other groups, the functionality of the electrodes remained intact. The PSE successfully recorded neural signals *in vivo* over the course of a month-long implantation, indicating that the techniques utilized in the production of the PSE can be used for the fabrication of future generations of 3D polymer neural probes.

ACKNOWLEDGMENT

The authors thank Drs. Curtis D. Lee, Christian A. Gutierrez, and Tuan Q. Hoang for their assistance on the project, Dr. Victor Pikov at the Huntington Medical Research Institutes (HMRI, Pasadena, CA 91105) for his insight and advice, as well as Dr. Donghai Zhu (USC) and the members of the Biomedical Microsystems Laboratory for their support.

REFERENCES

[1] D. H. Szarowski *et al.*, "Brain responses to micro-machined silicon devices," *Brain Res.*, vol. 983, nos. 1–2, pp. 23–35, Sep. 2003.

[2] T. Saxena *et al.*, "The impact of chronic blood–brain barrier breach on intracortical electrode function," *Biomaterials*, vol. 34, no. 20, pp. 4703–4713, 2013.

[3] V. S. Polikov, P. A. Tresco, and W. M. Reichert, "Response of brain tissue to chronically implanted neural electrodes," *J. Neurosci. Methods*, vol. 148, no. 1, pp. 1–18, Oct. 2005.

[4] R. Biran, D. C. Martin, and P. A. Tresco, "The brain tissue response to implanted silicon microelectrode arrays is increased when the device is tethered to the skull," *J. Biomed. Mater. Res. A*, vol. 82, no. 1, pp. 169–178, 2007.

[5] G. C. McConnell, H. D. Rees, A. I. Levey, C. A. Gutekunst, R. E. Gross, and R. V. Bellamkonda, "Implanted neural electrodes cause chronic, local inflammation that is correlated with local neurodegeneration," *J. Neural Eng.*, vol. 6, no. 5, pp. 056003-1–056003-12, 2009.

[6] J. Subbaroyan, D. C. Martin, and D. R. Kipke, "A finite-element model of the mechanical effects of implantable microelectrodes in the cerebral cortex," *J. Neural Eng.*, vol. 2, no. 4, pp. 103–113, 2005.

[7] P. Moshayedi *et al.*, "The relationship between glial cell mechanosensitivity and foreign body reactions in the central nervous system," *Biomaterials*, vol. 35, no. 13, pp. 3919–3925, 2014.

[8] J. K. Nguyen *et al.*, "Mechanically-compliant intracortical implants reduce the neuroinflammatory response," *J. Neural Eng.*, vol. 11, no. 5, p. 056014, 2014.

[9] R. Biran, M. D. Noble, and P. A. Tresco, "Directed nerve outgrowth is enhanced by engineered glial substrates," *Experim. Neurol.*, vol. 184, no. 1, pp. 141–152, 2003.

[10] J. Bartels *et al.*, "Neurotrophic electrode: Method of assembly and implantation into human motor speech cortex," *J. Neurosci. Methods*, vol. 174, no. 2, pp. 168–176, Sep. 2008.

[11] A. Mercanzini *et al.*, "Demonstration of cortical recording using novel flexible polymer neural probes," *Sens. Actuators A, Phys.*, vol. 143, no. 1, pp. 90–96, May 2008.

[12] P. J. Rousche, D. S. Pellinen, D. P. Pivin, Jr., J. C. Williams, and R. J. Vetter, and D. R. Kipke, "Flexible polyimide-based intracortical electrode arrays with bioactive capability," *IEEE Trans. Biomed. Eng.*, vol. 48, no. 3, pp. 361–371, Mar. 2001.

[13] Z. Xiang *et al.*, "Ultra-thin flexible polyimide neural probe embedded in a dissolvable maltose-coated microneedle," *J. Micromech. Microeng.*, vol. 24, no. 6, p. 065015, 2014.

[14] Y.-Y. Chen *et al.*, "Design and fabrication of a polyimide-based microelectrode array: Application in neural recording and repeatable electrolytic lesion in rat brain," *J. Neurosci. Methods*, vol. 182, no. 1, pp. 6–16, 2009.

[15] S. Takeuchi, D. Ziegler, Y. Yoshida, K. Mabuchi, and T. Suzuki, "Parylene flexible neural probes integrated with microfluidic channels," *Lab Chip*, vol. 5, no. 5, pp. 519–523, 2005.

[16] V. Castagnola *et al.*, "Parylene-based flexible neural probes with PEDOT coated surface for brain stimulation and recording," *Biosensors Bioelectron.*, vol. 67, pp. 450–457, May 2015.

[17] A. Tooker *et al.*, "Microfabricated polymer-based neural interface for electrical stimulation/recording, drug delivery, and chemical sensing—Development," in *Proc. 35th Annu. Int. Conf. IEEE Eng. Med. Biol. Soc. (EMBC)*, Jul. 2013, pp. 5159–5162.

[18] P. J. Gilgunn *et al.*, "An ultra-compliant, scalable neural probe with molded biodissolvable delivery vehicle," in *Proc. IEEE 25th Int. Conf. Micro Electro Mech. Syst. (MEMS)*, Jan./Feb. 2012, pp. 56–59.

[19] C. Y. Shih, T. A. Harder, and Y. C. Tai, "Yield strength of thin-film Parylene-C," *Microsyst. Technol.*, vol. 10, no. 5, pp. 407–411, 2004.

[20] D. C. Rodger, W. Li, J. D. Weiland, M. S. Humayun, and Y.-C. Tai, "Flexible circuit technologies for biomedical applications," in *Proc. Int. Conf. Microtechnol. Med. Biol.*, Rijeka, Croatia, May 2013.

[21] S. F. Cogan, "Neural stimulation and recording electrodes," *Annu. Rev. Biomed. Eng.*, vol. 10, pp. 275–309, Apr. 2008.

[22] P. Takmakov, K. Ruda, K. S. Phillips, I. S. Isayeva, V. Krauthamer, and C. G. Welle, "Rapid evaluation of the durability of cortical neural implants using accelerated aging with reactive oxygen species," *J. Neural Eng.*, vol. 12, no. 2, p. 026003, 2015.

[23] A. Tooker *et al.*, "Towards a large-scale recording system: Demonstration of polymer-based penetrating array for chronic neural recording," in *Proc. 36th Annu. Int. Conf. IEEE Eng. Med. Biol. Soc. (EMBC)*, Aug. 2014, pp. 6830–6833.

[24] F. Wu, L. W. Tien, F. Chen, J. D. Berke, D. L. Kaplan, and E. Yoon, "Silk-backed structural optimization of high-density flexible intracortical neural probes," *J. Microelectromech. Syst.*, vol. 24, no. 1, pp. 62–69, Feb. 2015.

[25] T. D. Y. Kozai *et al.*, "Chronic tissue response to carboxymethyl cellulose based dissolvable insertion needle for ultra-small neural probes," *Biomaterials*, vol. 35, no. 34, pp. 9255–9268, 2014.

[26] S. A. Hara *et al.*, "Pre-implantation electrochemical characterization of a Parylene C sheath microelectrode array probe," in *Proc. Annu. Int. Conf. IEEE Eng. Med. Biol. Soc. (EMBC)*, Aug./Sep. 2012, pp. 5126–5129.

[27] J. T. W. Kuo *et al.*, "Novel flexible Parylene neural probe with 3D sheath structure for enhancing tissue integration," *Lab Chip*, vol. 13, no. 4, pp. 554–561, 2013.

[28] D. C. Rodger *et al.*, "Flexible microfabricated Parylene multielectrode arrays for retinal stimulation and spinal cord field modulation," in *Proc. 4th Int. IEEE-EMBS Special Topic Conf. Microtechnol. Med. Biol.*, 2006, pp. 31–34.

[29] R. Patrick von Metzen and T. Stieglitz, "The effects of annealing on mechanical, chemical, and physical properties and structural stability of Parylene C," *Biomed. Microdevices*, vol. 15, no. 5, pp. 727–735, Oct. 2013.

[30] J.-M. Hsu, L. Rieth, S. Kammer, M. Orthner, and F. Solzbacher, "Effect of thermal and deposition processes on surface morphology, crystallinity, and adhesion of Parylene-C," *Sensors Mater.*, vol. 20, no. 2, pp. 87–102, 2008.

[31] A. Petrossians, J. J. Whalen, III, J. D. Weiland, and F. Mansfeld, "Electrodeposition and characterization of thin-film platinum-iridium alloys for biological interfaces," *J. Electrochem. Soc.*, vol. 158, no. 5, pp. D269–D276, 2011.

[32] D. T. Sawyer, "Voltammetric indicator electrodes," in *Experimental Electrochemistry for Chemists*. Hoboken, NJ, USA: Wiley, 1974, pp. 60–100.

[33] R. A. Illsley, S. G. Roscoe, E. D. Jackson, and T. J. Hughes, "An electrochemical investigation of the fouling of a model surface by a coliform bacterium," *Biofouling, J. Bioadhesion Biofilm Res.*, vol. 11, no. 3, pp. 191–199, 1997.

[34] M. Okochi, N. Nakamura, and T. Matsunaga, "Electrochemical control of bacterial cell accumulation on submerged glass surfaces," *Clean Products Process.*, vol. 1, no. 1, pp. 53–59, 1998.

[35] K. J. Otto, M. D. Johnson, and D. R. Kipke, "Voltage pulses change neural interface properties and improve unit recordings with chronically implanted microelectrodes," *IEEE Trans. Biomed. Eng.*, vol. 53, no. 2, pp. 333–340, Feb. 2006.

[36] I. Ulbert, E. Halgren, G. Heit, and G. Karmos, "Multiple microelectrode-recording system for human intracortical applications," *J. Neurosci. Methods*, vol. 106, no. 1, pp. 69–79, 2001.

[37] L. Grand *et al.*, "A novel multisite silicon probe for high quality laminar neural recordings," *Sens. Actuators A, Phys.*, vol. 166, no. 1, pp. 14–21, 2011.

[38] D. Zhan, J. Velmurugan, and M. V. Mirkin, "Adsorption/desorption of hydrogen on Pt nanoelectrodes: Evidence of surface diffusion and spillover," *J. Amer. Chem. Soc.*, vol. 131, no. 41, pp. 14756–14760, 2009.

[39] A. J. Bard and L. R. Faulkner, *Electrochemical Methods: Fundamentals and Applications*, 2nd ed. Hoboken, NJ, USA: Wiley, 2001.

[40] A. N. Frumkin, "Hydrogen overvoltage and adsorption phenomena—2," in *Advances in Electrochemistry and Electrochemical Engineering*, vol. 3. Hoboken, NJ, USA: Wiley, 1962, pp. 287–391.
[41] K. D. Wise, J. B. Angell, and A. Starr, "An integrated-circuit approach to extracellular microelectrodes," *IEEE Trans. Biomed. Eng.*, vol. BME-17, no. 3, pp. 238–247, Jul. 1970.
[42] D. F. Bahr, D. A. Crowson, J. S. Robach, and W. W. Gerberich, "The effects of residual stress on modulus measurements by indentation," in *Proc. 7th Thin-Films-Stresses Mech. Properties Symp.*, 1997, pp. 85–90.
[43] V. Branger, V. Pelosin, K. F. Badawi, and P. Goudeau, "Study of the mechanical and microstructural state of platinum thin films," *Thin Solid Films*, vol. 275, nos. 1–2, pp. 22–24, 1996.
[44] J. P. Seymour and D. R. Kipke, "Neural probe design for reduced tissue encapsulation in CNS," *Biomaterials*, vol. 28, no. 25, pp. 3594–3607, 2007.
[45] D. Loveday, P. Peterson, and B. Rodgers, "Evaluation of organic coatings with electrochemical impedance spectroscopy—Part 2: Application of EIS to coatings," *JCT Coatingstech*, vol. 1, no. 10, pp. 88–93, Oct. 2004.
[46] J. E. B. Randles, "Kinetics of rapid electrode reactions [with discussion]," *Discussions Faraday Soc.*, vol. 1, pp. 11–50, Mar. 1947.
[47] E. T. McAdams, A. Lackermeier, J. A. McLaughlin, D. Macken, and J. Jossinet, "The linear and non-linear electrical properties of the electrode-electrolyte interface," *Biosensors Bioelectron.*, vol. 10, nos. 1–2, pp. 67–74, 1995.
[48] W. Franks, I. Schenker, P. Schmutz, and A. Hierlemann, "Impedance characterization and modeling of electrodes for biomedical applications," *IEEE Trans. Biomed. Eng.*, vol. 52, no. 7, pp. 1295–1302, Jul. 2005.
[49] B. J. Kim *et al.*, "3D Parylene sheath neural probe for chronic recordings," *J. Neural Eng.*, vol. 10, no. 4, p. 045002, 2013.

Seth A. Hara received the B.S. degree in engineering from Swarthmore College, Swarthmore, in 2008, and the M.S. degree in biomedical engineering from the University of Southern California, Los Angeles, in 2013, where he is currently pursuing the Ph.D. degree in biomedical engineering with the Biomedical Microsystems Laboratory. His research interests are in the development of implantable Parylene-based microelectromechanical systems devices, in particular, on the electrochemical characterization and reliability of Parylene-based electrodes. He was a recipient of the NSF Graduate STEM Fellowship in K-12 Education in 2013.

Brian J. Kim received the B.S. degree double majoring in biomedical engineering and mathematics from Duke University, Durham, and the M.S. degree in biomedical engineering from the University of Southern California (USC), Los Angeles, in 2010 and 2013, respectively, where he is currently pursuing the Ph.D. degree in biomedical engineering (Provost's Ph.D. Fellow) with the Biomedical Microsystems Laboratory. His research interests are in the development of Parylene-based microelectromechanical systems devices for intracortical applications, in particular, on implantable Parylene-based sensor systems. He was a recipient of the Howard G. Clark Award for Independent Research from Duke University, the Viterbi School of Engineering Early Ph.D. Fellowship, and the USC Provost's Ph.D. Fellowship.

Jonathan T. W. Kuo received the B.S. degree in bioengineering from the University of California at San Diego, in 2007, and the Ph.D. degree in biomedical engineering from the University of Southern California, Los Angeles, in 2013. He was a recipient of the Viterbi Dean's Doctoral Fellowship during his graduate studies.

Ellis Meng (M'02–SM'09) received the B.S. degree in engineering and applied science, and the M.S. and Ph.D. degrees in electrical engineering from the California Institute of Technology (Caltech), Pasadena, in 1997, 1998, and 2003, respectively. She has been a Professor with the Department of Biomedical Engineering, University of Southern California, Los Angeles, since 2004. She currently holds a joint appointment with the Ming Hsieh Department of Electrical Engineering. Her research interests include bioMEMS, implantable biomedical microdevices, microfluidics, multimodality integrated microsystems, and packaging. She held the Viterbi Early Career Chair in the Viterbi School of Engineering. She is a Member of Tau Beta Pi, the Biomedical Engineering Society, the Society of Women Engineers, and the American Society for Engineering Education. She was a recipient of the Intel Women in Science and Engineering Scholarship, the Caltech Alumni Association Donald S. Clark Award, and the Caltech Special Institute Fellowship. She has also received the NSF CAREER and Wallace H. Coulter Foundation Early Career Translational Research Awards. In 2009, she was recognized as one of the TR35 Technology Review Young Innovators under 35.